Summer 8-1-2022

Characterization of the Surficial Aquifer System for Non-potable Use at the Wormsloe Historic Site, Chatham County, Georgia.

Kolawole Arowoogun

Characterization of the Surficial Aquifer System for Non-potable Use at the Wormsloe Historic Site, Chatham County, Georgia.

by

Kolawole Arowoogun

Under the Direction of Brian Meyer, PhD

A Thesis Submitted in Partial Fulfillment of the Requirements for the Degree of

Master of Science

in the College of Arts and Sciences

Georgia State University

2022

ABSTRACT

The surficial aquifer system at the Wormsloe State Historic site has the potential to serve as an alternate groundwater source for non-potable water needs in Georgia. This study integrates ground penetrating radar (GPR), digital elevation model (DEM) derived from Light Detection and Ranging (LiDAR), hydrograph data, and porosity estimates to evaluate the total water storage and change in storage. The GPR data mapped the depth to the confining layer and the water table depth. The magnitude of seasonal fluctuations in hydraulic head was extracted from hydrograph data. These datasets were used to construct a water table elevation map for two seasonal conditions. Porosity estimate from the repacked samples was integrated and used to compute total water storage and the changes in storage. This study shows that the surficial aquifer is an alternate groundwater source but limited by seasonal fluctuation in water storage and lateral and inland saltwater intrusion.

INDEX WORDS: Ground penetrating radar, Shallow groundwater, Irrigation, LiDAR

Characterization of the Surficial Aquifer System for Non-potable use at the Wormsloe Historic Site, Chatham County, Georgia.

by

Kolawole Arowoogun

Committee Chair: Brian Meyer

Committee: Luke Pangle

Hassan Babaie

Electronic Version Approved:

Office of Graduate Services

College of Arts and Sciences

Georgia State University

August 2022

DEDICATION

The project is dedicated to the support of my family, friends, and mentors.

ACKNOWLEDGEMENTS

I acknowledge and offer sincere gratitude to my advisor Dr. Brian Meyer for his guidance and insights during the collection of data and subsequent analysis and formal writing of this thesis. I also wish to appreciate Dr. Luke Pangle for his input. Gratitude is due to Dr. Hassan Babaie who served as a member of my thesis committee for devoting his time and energy to this project.

In addition, I wish to acknowledge my classmate, Donata Borsos, who volunteered to join me in the field during the GPR data acquisition. Sincere appreciation is due to Wormsloe Foundation and Wormsloe Institute for Environmental History, most especially Sarah Ross for her creating an enabling environment during the data collection. Lastly, I want to use the opportunity to appreciate Mr. Oluseun Sanuade and Dr. Sarah Ledford for their guidance and mentorship during my study at Georgia State University.

TABLE OF CONTENTS

ACKNOWLEDGEMENTS V

LIST OF TABLES VIII

LIST OF ABBREVIATIONS X

1 INTRODUCTION 1

1.1 Significance of the study 2

1.2 Research Questions 3

1.3 Research Objectives 3

1.4 Basic Principle of GPR in Hydrology 3

1.4.1 Data display 6

1.4.2 Interpretation of hydrological features from GPR data 7

2 DESCRIPTION AND GEOLOGICAL SETTING OF THE STUDY AREA 9

2.1 Location and description of the study area 9

2.2 Geology and hydrological settings of the study area 10

3 METHODS 12

3.1 GPR data acquisition and correction 12

3.2 Soil sample analysis 18

3.3 Water table, water table elevation and total water storage estimation 20

3.4 Aquifer recharge 22

4 RESULTS 23

4.1 Hydrogeological framework 23

4.2 Porosity estimate 24

4.3 Total availability of water and annual recharge 25

5 DISCUSSION 31

5.1 Surficial aquifer hydrogeological framework 31

5.2 Total availability of water and annual recharge estimates 32

5.3 Future research/Limitation of data 34

6 CONCLUSIONS 35

REFERENCES 36

LIST OF TABLES

Table 1.1: Bulk dielectric of constant of common earth material (modified after Daniels, 1996). 5

Table 3.1: Summary of GPR profile length in the study location 15

Table 3.2: GPR data acquisition parameter 16

Table 3.3: GPR calibration velocity data for transforming two-way time to depth scale. 18

Table 4.1: Statistical distribution of the depth to confining layer mapped on the GPR profiles .. 23

Table 4.2: Summary of the porosity testing results of the repacked samples. 25

Table 4.3: Summary of total water storage and percentage change in storage. 30

Table 4.4: Summary of change in water level and annual recharge estimate between 2016-2017.

..... 31

LIST OF FIGURES

Figure 1.1: Schematic diagram illustrating the application of ground penetrating radar system (Healy et al. 2006)..... 4

Figure 1.2: GPR image showing water table depth in unsaturated sands. The water table surface appears as a distinct reflector (Doolittle et al. 2006). 8

Figure 2.1 Map showing the location of the study area (Williams, 2019)..... 9

Figure 2.2: Accessibility map of the study area..... 10

Figure 3.1: Field layout of GPR profile lines and MWs across the study location. 12

Figure 3.2: Towed GPR field set up for data collection in the study area. The antennae is dragged through the study area, the receiver records and stores the signal on the GSSI-SIR 4000 display unit placed in the moving utility vehicle. 14

Figure 4.1: Box and whisker plot showing the statistical distribution of the depth to the confining layer extracted from the GPR data in the study area. 24

Figure 4.2: Estimated water-table elevation constructed from LiDAR and GPR data for Wormsloe Historic site. 26

Figure 4.3: Long-term water level data from Wormsloe site Level transducer (Hodges, 2019). The water levels were recorded in MW-02 from 2016 -2018. 27

Figure 4.4: Seasonal high water table (SHWT) map of Wormsloe Historic site..... 28

Figure 4.5: Seasonal low water table (SLWT) map of Wormsloe Historic site. 29

Figure 5.1: Processed GPR data from the 2021 data acquisition at Wormsloe site depicting the surficial aquifer system configuration and the accompanying signal attenuation recorded on the GPR section..... 32

LIST OF ABBREVIATIONS

ACF: Apalachicola-Chattahoochee-Flint

DEM: Digital elevation model

GPR: Ground penetrating radar

LFA: Lower Floridan Aquifer

LIDAR: Light detection and ranging

MHZ: Mega Hertz

MW: Monitoring well

SHWT: Seasonal high water table

SLWT: Seasonal low water table

UFA: Upper Floridan Aquifer

1 INTRODUCTION

The United States (U.S.) has ecologically diverse and productive coastal regions which are important to their economic growth. Coastal counties account for about 40% of the nation's total population and include notable cities and rapidly evolving counties (Wilson and Fischetti, 2010; Hodges, 2019). Although these regions have abundant water resources owing to their favorable subtropical climate, the Southeastern U.S. has seen an increase in frequency and intensity of droughts in recent times, especially in agricultural areas (Engstrom et al., 2021).

Due to the increased frequency of drought, there has been a noticeable decrease in water reservoirs and an accompanying water shortage. The consequence of these water shortages have manifested in interstate conflicts and litigation. The high demand and corresponding water shortage has led to the legal conflict between Alabama, Florida and Georgia in a war termed the 'Tri State water wars' (Jordan, 2001). The conflict borders around the Apalachicola-Chattahoochee-Flint (ACF) River basin, shared by Alabama, Florida, and Georgia. ACF basin has witnessed a decline due to Georgia's increasing water need for its agricultural activities. This situation has allegedly affected Florida's Oyster business and ecosystem due to declining water discharged into the area (Lancaster, 2017).

Georgia's population will continue to increase; it is projected to increase by approximately 42% in 2030 (Painter, 2019). Therefore, natural resources are necessary to support these populations, as people will need water for various industrial, agricultural, and recreational purpose (Osinowo and Arowoogun, 2020). But surface water sources from river basins are insufficient to meet the increasing water demand due to vulnerability to contamination and reported large scale drought which reduce water availability (Zowam, 2020)

Therefore, harnessing groundwater is a vital alternative. However, Georgia's freshwater supply is heavily reliant on water withdrawal from the Upper Floridan Aquifer (UFA). The UFA is a major aquifer system in the US (Karki et al. 2021), but it is shared by neighboring states of Alabama, Florida, Mississippi, and South Carolina (Marella and Berndt, 2005). In addition, in some areas, the UFA is too deep, and its development may not prove to be economical (Marella, 2009). Also, karst features have developed in areas where the UFA is unconfined, this makes it more prone to contamination from pesticides and nitrates, since most of these areas are agricultural regions (Berndt et al., 2014).

In coastal Georgia where this study was conducted, over pumping of groundwater from the UFA has led to the formation of a regional cone of depression which allows saltwater to move laterally within the aquifer (Falls et al., 2005; Reichard et al., 2014). The influx of saltwater contamination has forced the Georgia Environmental Protection Division (GaEPD) to develop conservation efforts aimed at limiting deeper groundwater exploitation in parts of the coastal area (Clarke, 2003). Thus, to offset the deficit in the water demand due to the conservation efforts, there is a need for an alternative water supply that can be harnessed to meet non-potable water demands. In this regard, the surficial aquifer system is considered as an untapped groundwater resource that can be harnessed to meet residential and landscape irrigation in the area. This study therefore attempts to understand the geometry of the surficial aquifer and compute groundwater storage and accompanying changes due to seasonal fluctuations.

1.1 Significance of the study

The development of the surficial aquifer will enhance the sound management of water resources. In addition, it will promote sustainable use of water resources and reduce the reliance on the UFA and surface water sources. This research will further inform the public that the surficial

aquifer system is an alternative water sources that can be harnessed to meet residential and small-scale agricultural irrigation demand.

1.2 Research Questions

This research seeks to provide answers to salient questions on the surficial aquifer systems. It, however, revolves around the three interwoven fundamental questions.

1. Can GPR map the depth to the water table and the confining layer of the surficial aquifer system across the area?
2. What is the approximate total water storage in the surficial aquifer system in the study area?
3. What is the magnitude of the change in the total water storage in the surficial aquifer under seasonal high-water table (SHWT) and seasonal low water table (SLWT) conditions?

1.3 Research Objectives

The research is aimed at estimating the total water storage in the surficial aquifer system. It will also evaluate limitations in the amount of available water including seasonal controls and saltwater intrusion that affects water quality.

1.4 Basic Principle of GPR in Hydrology

GPR is a non-destructive geophysical method that uses the scattering principle of electromagnetic waves to map subsurface features (Leucci and Negri, 2006). It operates on the principle of transmitting electromagnetic energy from an antenna into the subsurface (Holden et al. 2002). The resulting waves from the receiving antennae are recorded (Figure 1.1).

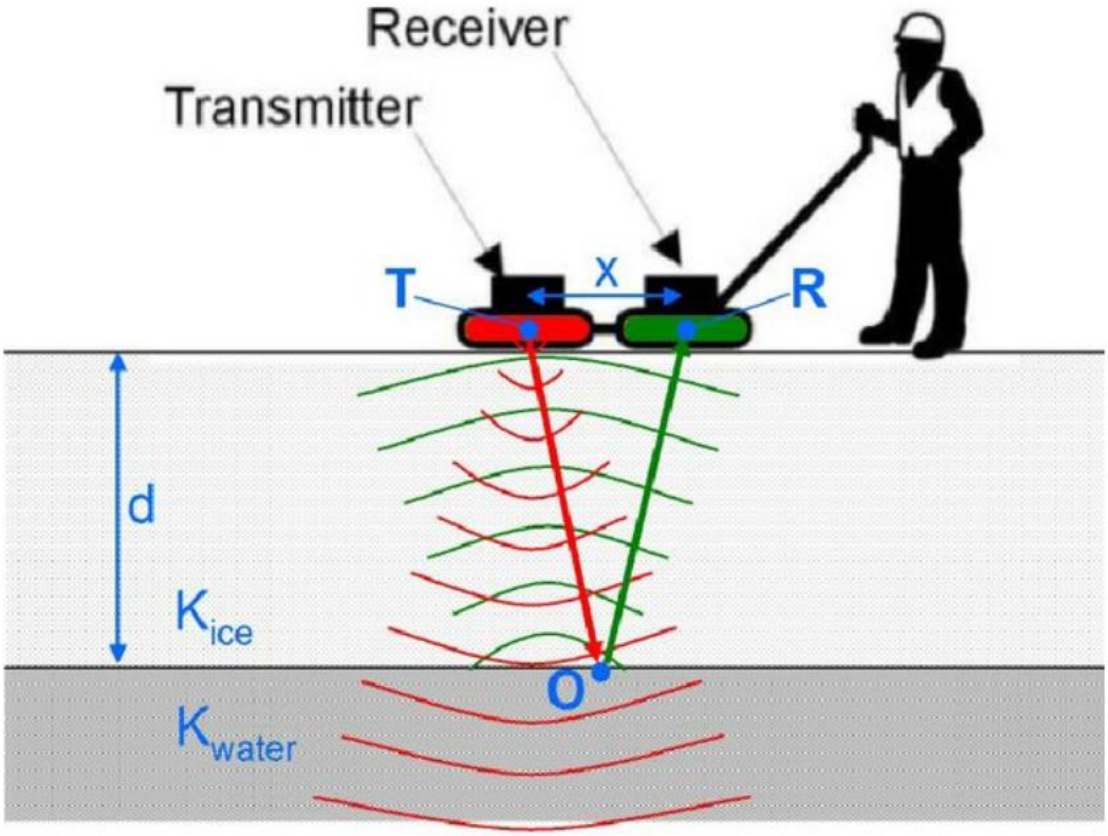

Figure 1.1: Schematic diagram illustrating the application of ground penetrating radar system (Healy et al. 2006).

The wave velocity propagation of GPR is controlled by dielectric permittivity. Dielectric permittivity has both real and imaginary component. The real portion is the dielectric constant; it is the ratio of the electric-field storage capacity of earth material compared to free space (Martinez and Byrnes, 2001).

The imaginary portion is expressed as dielectric loss, and it represent the dispersion and attenuation. In poorly conductive material (usually less 10 mS/m), the dielectric loss is often negligible, and since most geological material have conductivity below 10 mS/m (Martinez and Brynes, 2001). Therefore, the dielectric constant is the main measured component of dielectric permittivity (Martinez and Byrnes, 2001). Although the dielectric constant typically decreases with

increasing frequencies but has a consistent value over a wide range usually between 25 -1500 MHZ (Martinez and Byrnes, 2001). Therefore, having knowledge of dielectric constant values of earth material aids the planning of GPR data collection. The dielectric constant values of common geologic materials are presented in Table 1.1.

Table 1.1: Bulk dielectric of constant of common earth material (modified after Daniels, 1996).

Material	Dielectric constant
Air	1
Freshwater	81
Fresh water ice	4
Sea water ice	4-8
Snow	8-12
Permafrost	4-8
Sand, dry	4-6
Sand, wet	10-30
Limestone wet	7
Limestone dry	8
Shale, wet	6-9
Clay, dry	2-6
Clay, wet	15-40
Soil, sandy dry	4-6
Soil, sandy wet	15-30
Soil, loamy dry	4 -6
Soil, loamy wet	10-20
Soil Clayey wet	10-15
Coal dry	8
Granite, wet	7
Granite, dry	5
Salt, dry	4 -7

The dielectric permittivity is affected by the variation in bulk density of materials and water content (Guo et al. 2012). Therefore, due to permittivity contrast, different geological material maybe reflected and /or scattered on GPR (Annan, 2005). The reflection or scattering is because when a wave encounters earth material with different permittivity, the electromagnetic energy will change in direction and velocity.

When radar waves travel across the interface between media with different electrical and magnetic material, portion of energy are reflected to the surface and recorded by the receiving antenna while the remaining energy continue to travel until the amplitude of the signal dies off (Martinez and Brynes, 2001). Thus, when travelling through media, the radar energy decays significantly with time (Neto and de Medeiros, 2006). As a result, the GPR is primarily suited for near-surface studies (Conyers, 2004).

The resolution of GPR is primarily a function of the antennae frequency, conductivity of the geologic medium and the penetration depth (Paz et al. 2017). Therefore, in saline media and clay-rich environment; there is a signal loss due to high conductivity in through a phenomenon known as signal attenuation.

1.4.1 Data display

The aim of GPR survey is to produce a final output of GPR data that approximate the subsurface geology and image the anomalies of interest. Therefore, data display is crucial to GPR data interpretation. GPR data can be displayed as 1D trace, 2D cross section and a 3D block.
The 1D trace is the recording of pulses from transmitting antennae to the receiver over a period, and it is the building block of all display (Martinez and Byrnes, 2001). When a color scale or gray scale is applied to the amplitude values of a trace it is called a scan. The 2D trace consist of aggregated traces to produce a 2D cross section.

3D display is a block view of GPR which consists of stacks of 2D traces recorded at different spatial location on the surface (Martinez and Byrnes, 2001). For accurate interpretation, GPR data are best recorded on a 3D display. The 3D arrangement helps in optimizing GPR signals. Thus, reducing the noise to signal ratio and make target more easily identifiable (Daniels et al. 1997).

1.4.2 Interpretation of hydrological features from GPR data.

Interpretation of GPR data is highly subjective and requires expert judgement (Annan, 2005). Accurate interpretation of GPR often use in-situ well data or core sample for constraining lithologic inference in hydrological studies.

The GPR radar typically takes measurement in time scale and produce a time-distance record. The vertical time scale represents the two-way travel time of the radar wave through the earth. However, since geologic observations are best measured on a distance scale (Doolittle et al. 2006). The time scale can be transformed using the velocity of pulse propagation known as the calibration velocity. The calibration velocity data is best estimated by measuring two-way travel time of a known reflector to a measured or known depth (Doolittle et al. 2006). The velocity is expressed using the equation 1 (Daniels, 2004).

- Velocity (V) = 2*D/T (1)

Where, V = velocity of wave through a geologic material

D = depth from the surface

T = two-way travel time of the radar wave

The velocity and the distance relationship expressed in the equation above are used to convert time scale into depth scale for evaluating water table depth in hydrology (Doolittle et al. 2006).

Water table depth estimate is one of the key hydrological information that can be extracted from the GPR data (Smith et al. 1992). Generally, the top of the saturated zone represents a clear

and continuous reflector from the subsurface on the radar image, thereby enabling mapping of water table (Figure 1.2)

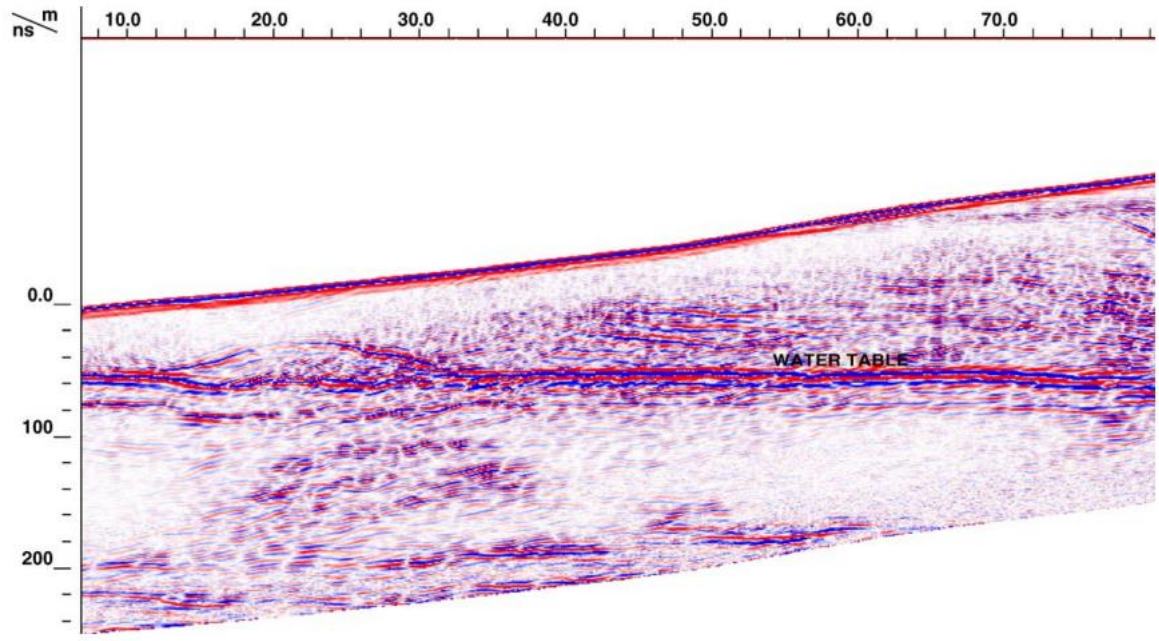

Figure 1.2: GPR image showing water table depth in unsaturated sands. The water table surface appears as a distinct reflector (Doolittle et al. 2006).

However, the strength of the reflector depends on the sharpness of the boundary and the difference in electrical properties that exist between the saturated zone and the unsaturated zone (Johnson, 1992). Thus, locating water table depth using the GPR requires some level of skills and knowledge of the subsurface geology because GPR signals differs from one geologic medium to another. For instance, the water table in coarse textured material due to the sharp contrast in the water content produces a strong and identifiable reflections on radar image.

2 DESCRIPTION AND GEOLOGICAL SETTING OF THE STUDY AREA

2.1 Location and description of the study area

The study area is on the southern part of the Isle of Hope within the Wormsloe State Historic Site (Wormsloe), about 10 miles from downtown Savannah, Chatham County, Georgia (Figure 2.1).

Figure 2.1 Map showing the location of the study area (Williams, 2019).

Wormsloe spans 822-acres and is accessed by minor unimproved roads and hiking trails. The area is characterized by maritime forest, tidal marshes, and tidal river channels (Figure 2.2). The study area has an average elevation of 13 feet above the mean sea level (Williams, 2019).

Areas of low elevation in the study area have served as drinking water sources in the historical past (Bryan, 1753).

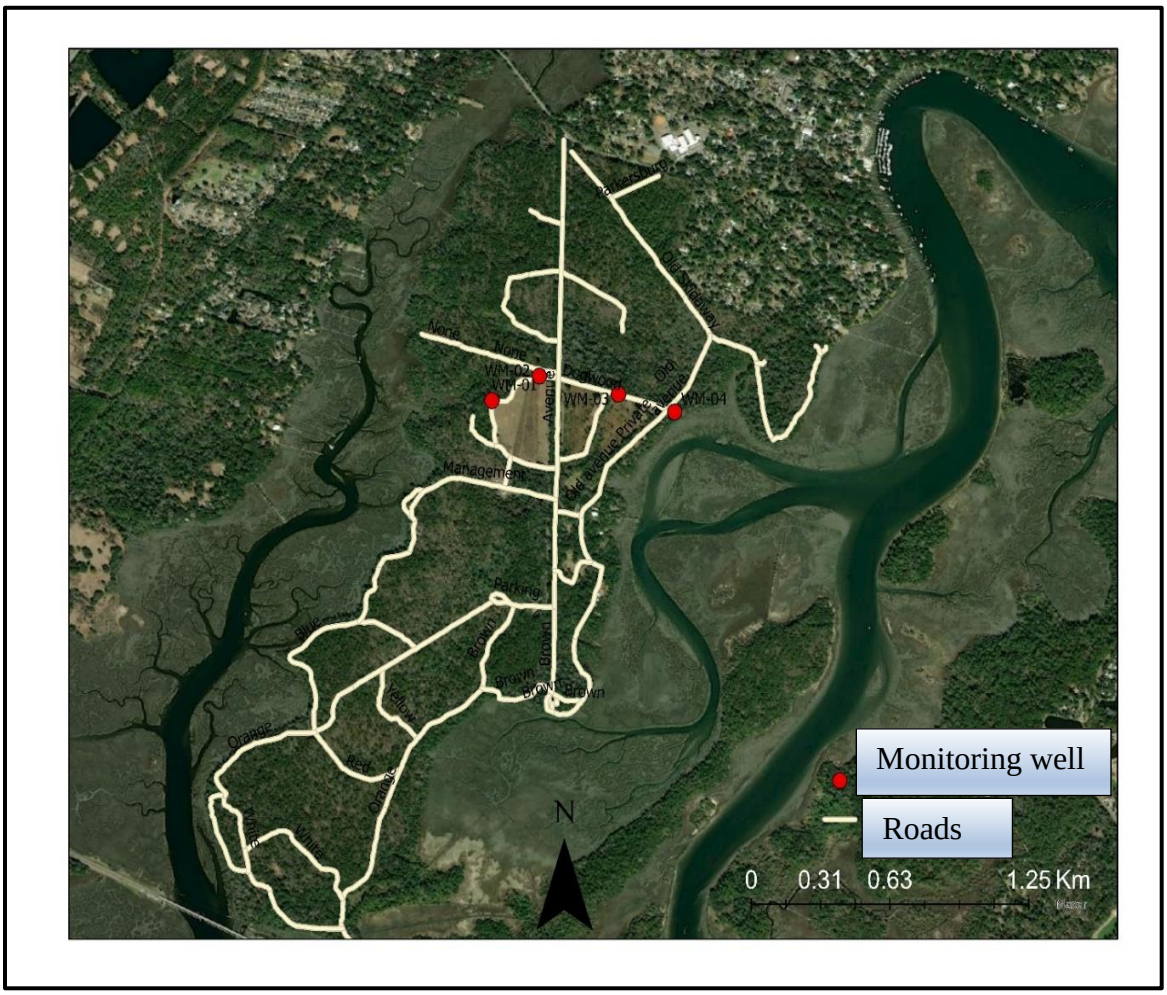

Figure 2.2: Accessibility map of the study area.

2.2 Geology and hydrological settings of the study area

Georgia's geology is comprised of five distinct physiographic provinces based on the geologic age, structures, landforms, and rock assemblages. These regions include the Appalachian Plateau, Valley and Ridge, the Blue Ridge, the Piedmont, and the Coastal Plain (Cocker, 1999). The Wormsloe study area is located on the Isle of Hope and lies in the Coastal Plain province of

Georgia. This is the youngest and the largest of all the geologic provinces of the state and occupies all southern Georgia (Oladeni, 2022). It is characterized by an alternation of sand and clay lenses alongside variable composition of karstic rocks (limestone and dolomite) which range in age from the Paleocene to recent (Clarke et al. 2011).

In terms of hydrological setting, the study area has two main aquifer types, namely the unconfined surficial aquifer and the underlying confined UFA system. The surficial aquifers consist of interlayered lenses of sand, clay, and limestone beds of Miocene to Holocene (Clark, 2003). They are found to be under confined and unconfined conditions in various parts of the area depending on the clay thickness distribution (Reichard et al. 2014). Currently, the Wormsloe site has not harnessed its surficial aquifer system for potable needs, and it is reported to have reasonable volume of water to meet non-potable use (Williams, 2019).

The Floridan aquifer system is a collective name for the UFA and the Lower Floridan Aquifer (LFA) system. It is one of the most productive underground reservoirs in the US with a coverage of about 100,000 sq miles in areas which include Florida, parts of Georgia, Alabama, South Carolina, and Mississippi (Marella and Berndt, 2005; Barlow and Richard, 2009). The Floridan aquifer consist of Paleocene to Oligocene carbonate rocks (Cherry et al. 2015). The LFA is located at a much greater depth and is rarely penetrated by wells; in addition, it contains saline water intrusion which makes it unsuitable for potable uses.

The increasing rate of groundwater withdrawal in the study area is manifest in a head decline in the UFA near Savannah area. The head drop has led to the development of a cone of depression (Barlow and Richard, 2009). For example, Reichard et al. (2014) reported a cone of depression spanning over a 113 km diameter and an observed drop in the head with a magnitude

of approximately 40 m. The observed depression and head drop made this study area a target for saline water intrusion research.

3 METHODS

3.1 GPR data acquisition and correction

Ground penetrating radar (GPR) was used in the current study to evaluate the thickness of the shallow unit of the surficial aquifer system. Data used in this study were collected in 2021 led by Geoscience State University (GSU) Geosciences faculty (Dr. Meyer) and students (Kolawole Arowoogun and Donata Borsos). Additional GPR incorporated data were collected in 2018 by Dr. Meyer and Mr. Albert Killingsworth. The 2021 data were acquired across the study area by establishing profiles along unimproved roads and hiking trails within the site (Figure 3.1).

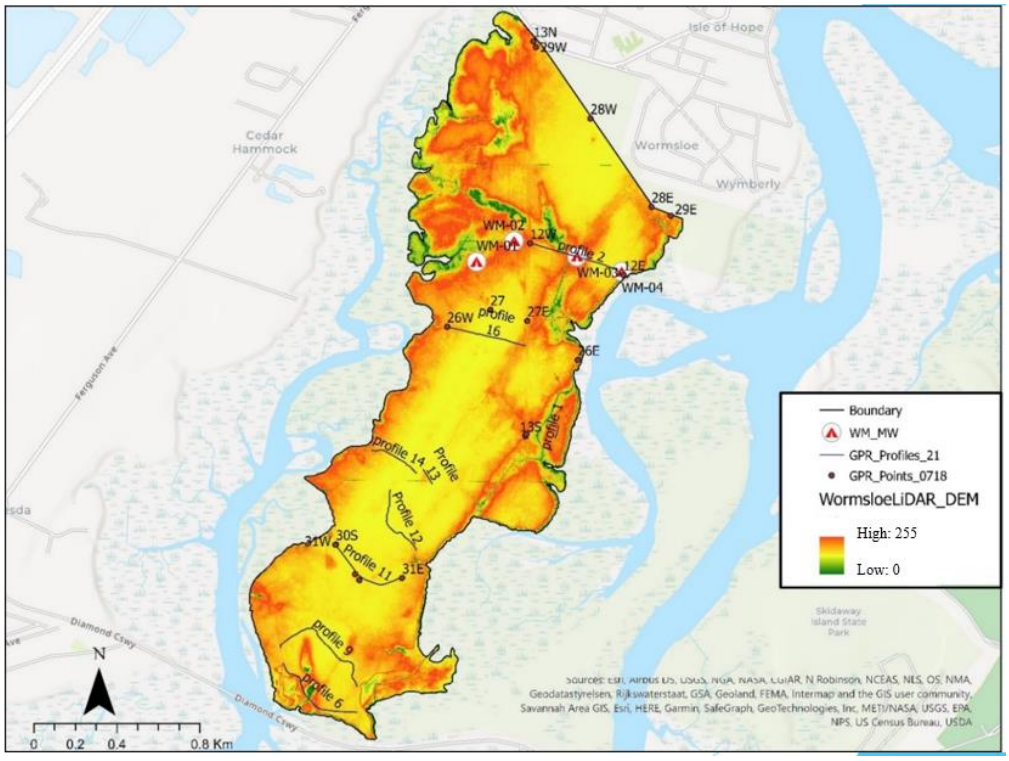

Figure 3.1: Field layout of GPR profile lines and MWs across the study location. The GPR data are displayed as point and profile lines. The field data and the monitoring wells are located on a digital elevation model.

For the 2021 data, the GPR systems was mounted behind a utility vehicle, and towed across the area at an average speed of 4 km/hr. The GPR unit was a Geophysical Survey Systems Incorporated (GSSI) Model No. 5106/A using 200 MHz antennae. The 2019 data was collected using a MALA Inc. GPR system with a Ramac X3M controller paired with 160 MHz antenna. Both systems use a shielded antennae that incorporates both transmitter and receiver in one unit at a fixed spacing and both systems use a wheel odometer to distinguish distance.

GPR profile locations were recorded using a Trimble GeoExplorer XH handheld GPS device accurate to within 0.15m. In the Coastal Plain of Georgia, dry sands are optimal for the use of GPR devices. Groundwater increases the dielectric constant and decreases velocity of radar waves. Saltwater saturation causes a loss of return signal and clay soils attenuate radar until it will not produce viable returns. The water table was identified by the change in velocity associated with the interface of unsaturated and water saturated sands (water table) and the underlying confining layer was identified as a hard reflector. The GPR system set up used for collecting the 2021 data is shown in Figure 3.2.

Figure 3.2: Towed GPR field set up for data collection in the study area. The antennae is dragged through the study area, the receiver records and stores the signal on the GSSI-SIR 4000 display unit placed in the moving utility vehicle.

The 200 MHZ and 160 MHZ antennae were chosen to provide a balance between the shallow target depth and higher resolution. Since GPR operates based on trade-off between depth of penetration and resolution, a mix of both 160 MHZ and 200 MHZ antennae provide a moderate resolution and depth penetration for mapping the surficial aquifer. The towed GPR survey was conducted along existing paths and roadways for collection. A total of nine (9) GPR profiles lines with varying lengths were acquired in the study area in 2021 (Table 3.1).

Table 3.1: Summary of GPR profile length in the study location

S/N	Profile ID	Length (Ft)	Length (m)
1	Profile 12	1209.25	368.58
2	Profile 11	1363.98	415.74
3	Profile 14	847.63	258.36
4	Profile 13	269.47	82.13
5	Profile 1	211.29	64.40
6	Profile 16	1280.86	390.41
7	Profile 9	1907.42	581.38
8	Profile 6	1567.40	477.74
9	Profile 2	1515.44	461.91
	Total length	**10172.74**	**3100.65**

The GPR data acquisition was conducted during November 2021. The GPR profiles were collected within two days, during which no rainfall event occurred, although there was precipitation a few days before the commencement of data acquisition that caused the movement of water into the edge of the marsh, thereby making certain areas inaccessible. Thus, we expect no serious temporal effect from drainage and precipitation that should affect the quality of the data collected.

Profiles were calibrated using known groundwater depths at the shallow monitoring wells at the Wormsloe study area. The GPR data were acquired in shallow profiling mode along the established traverse with a dielectric constant of 9, a set range at 150 ns, and traces consisting of 512 samples per scan. The 150 ns trace was discreetly sampled at the 16 bits per sample. The acquisition parameters are summarized in Table 3.2.

Table 3.2: GPR data acquisition parameter

Acquisition Parameter	Value
GPR System	SIR-4000
GPR System S/N	2007
Number of Channels	1
Scans/Sec	177.00
Scans/Unit	6.00
Samps /Scan	512
Bits / Sample	32
Dielectric Constant	6.00
Channel	1
Antenna Type	5106
Transmit Rate (KHz)	100
Position (nS)	-16.59
Range (ns)	165.91

The raw GPR data were subjected to variety of processing techniques using the commercial software Radan Version 7 developed by GSSI. The processing was performed to improve the signal to noise ratio and make it more meaningful for geologic interpretation (Porsani et al. 2012; Ganiyu et al., 2019). The zero-time correction is a major step in processing GPR data. It is applied to adjust the zero position of the first arrival signal by moving the trace down by a few nanoseconds, thereby ensuring accurate imaging of the depth (Essam et al., 2020). It also helps in eliminating the amplitude value of the signal and interpolates for each GPR trace (Maruddani and Sandi, 2019; Ciampoli et al. 2019). Background removal was applied to remove horizontal banding and clutter

noise data. This correction is achieved without diminishing the signal (Khan and Al-Nuaimy, 2010). The resulting data were filtered using the test filters to remove the noise and make target features more easily identifiable.

The GPR was able to map depth to the water table in the surficial aquifer due to observed velocity change at the interface of saturated and unsaturated zone (polarity reversal) and compared with preliminary groundwater model. The observed velocity change at the interface is due to increase in conductivity caused by the groundwater occurrence. Therefore, to accurately calculate the water table depth from the GPR profile there is a need to calibrate the velocity of the GPR signal. We used the water level depths and lithologic information of the existing monitoring wells in the area were used to validate the GPR interpretation results. The calibration velocity used in this study was adapted from the work of Ben Hodges (M.S. 2019), who had earlier conducted GPR surveys in the area. The calibration velocity data are presented in Table 3.3.

Table 3.3: GPR calibration velocity data for transforming two-way time to depth scale.

Date	Location	Profile ID	Velocity (ft/us)	Velocity (cm/ns)	Source
7/10/2018	MW-01	97	564	17.2	Water level measurement
7/10/2018	MW-02	99	539	16.4	(depth calibration)
7/10/2018	MW-03	102	538	16.4	Water level measurement
7/11/2018	Profile	119	434	13.2	(depth calibration)
7/12/2018	Profile	130	450	13.7	Water level measurement
7/16/2018	Profile	145	515	15.7	(depth calibration)
7/16/2018	Profile	161	418	12.7	Hyperbola fit
7/19/2018	MW-01	239	532	16.2	Hyperbola fit
7/19/2018	MW-02	240	490	14.9	Hyperbola fit
7/19/2018	MW-03	241	501	15.3	Hyperbola fit
		Minimum	418	12.7	Water level measurement
		Maximum	564	17.2	(depth calibration)
		Mean	498.1	15.2	Water level measurement
		Geometric Mean	495.8	15.1	(depth calibration)
		Median	508.0	15.1	Water level measurement
					(depth calibration)

3.2 Soil sample analysis

Repacked samples from the drilling of monitoring wells (MW03 and MW04) in the study area were collected to estimate the porosity of the surficial aquifer. The samples were collected from MW03 (depth of 9 ft and 12 ft) and MW04 at a depth of 15 ft (Figure 3.3).

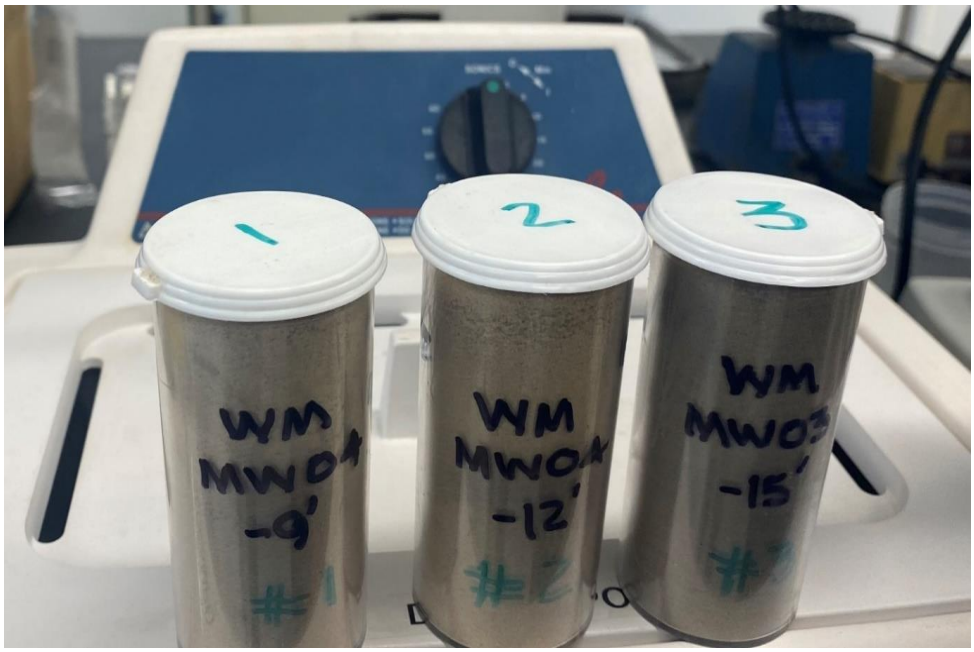

Figure 3.3: Repacked soil sample retrieved from monitoring wells in the study area to be used in estimating porosity of soil.

We analyzed collected samples in the laboratory at the Geosciences Department at Georgia State University, Atlanta. The porosity estimation experiment was conducted using the procedure summarized follows.

The samples collected were oven dried for about 24 hours at a temperature of about 60^{o}C to remove all moisture content. The samples collected from MW03, and MW04 were then weighed to obtain the dry mass of the samples. The volume of solid (Vs) was calculated by dividing the dry mass by the density of quartz (2.65 g/cm^{3}). Drops of water were slowly added to the sample and shaken to allow the water to fill to the base of the soil so that air can escape from the top. We repeated the process until no gas bubbles was coming out of the sample, and the soil samples were completely saturated, the mass of the saturated sample was recorded as

Mass $_{sat}$. The dry mass was subtracted from the saturated mass (Mass$_{sat}$) to calculate the mass of water. The porosity was calculated using equation 2.

- Porosity = $MASS_{water(g)}$ / VOL_{total} * 100 (2)

3.3 Water table, water table elevation and total water storage estimation

The water table is observed in coarse grained materials as a sharp reflector as result of changes in the propagation velocity as the wave travels through different media (dry pore spaces above the water table and saturated pore spaces below the water table) and are recorded as a reflector in GPR. This reflection results in an observed polarity reversal on the GPR profiles which occur as the velocity of the wave is slowed upon contact with saturated media (Figure 3.4).

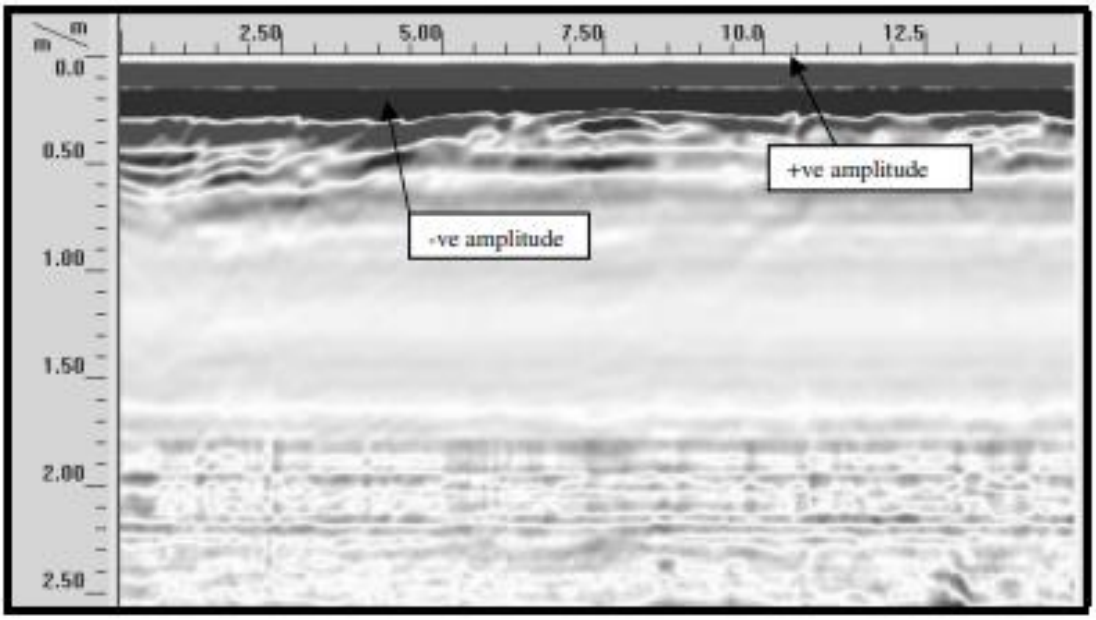

Figure 3.4 : GPR radargram showing the changes in polarity as the radar wave travels from media of higher velocity to lower velocity (polarity reversal). The zone of the change was interpreted as the water table location of the shallow aquifer (Makkawi, 2004).

The movement from unsaturated to saturated media causes a change in dielectric permittivity and propagation velocity, of these two media resulting in a polarity reversal. Therefore, the water table can be delineated on the radargram by identifying the zone of polarity reversal. The water table surface elevation was calculated at the GPR profile locations by

subtracting the surface topography from the 30-meter resolution digital elevation model (DEM) derived from the Light Detection and Ranging (LIDAR) data from the depth to groundwater obtained from the GPR.

- Water table Elevation (WT_{EL}) = Surface Elevation (LIDAR derived) - Groundwater depth (GPR derived) (3)

Equation 3 was implemented in ArcGIS Pro through the raster calculator function to estimate the water table elevation for individual pixels across the study area. The water table elevation was used to calculate the seasonal change in the water table (that is, seasonal high and low). The seasonal water table changes were obtained by subtracting the estimated water table elevation (from equation 2) from the hydraulic head drop recorded by the MW in the area.

- Seasonal water table change = Water table elevation (From Equation 1) – Hydraulic head change (Derived from hydrograph) (4)

The pixel-by-pixel estimation of the equation was performed using the raster calculator function in ArcGIS Pro version 2.9. The total water storage was estimated by calculating the volume of the saturated aquifer in the study area and multiplying the value with the mean porosity obtained from the laboratory analysis of the repacked soil sample. The algebraic operation involved in the estimation of total water storage was done using raster calculator and the total water storage calculation was performed using the surface volume tool as part of the 3D analyst extension in ArcGIS Pro.

3.4 Aquifer recharge

Groundwater recharge refers to the movement of water from the lower portion of the vadose zone into the water table (Freeze and Cherry, 1979; Sophocleous, 1991). The knowledge of groundwater recharge is essential in hydrologic studies, as it aids the management of groundwater systems and help protect the aquifer (Healy and Cook, 2002). Therefore, it is imperative to quantify the magnitude of quantification of recharge in an aquifer.

There are a variety of methods for quantifying groundwater recharge; such hydrograph analysis, water table fluctuation and many more (Jassas, 2014; Qablawi, 2016), each with its inherent limitations across spatial and temporal scales (Scanlon et al. 2002). The water table fluctuation (WTF) was applied this study due to its simplicity and suitability for measuring recharge in shallow unconfined aquifer (Healy and Cook, 2002). The method is premised on the assumption that water level rise is due to recharge, though other events such as earth tides and entrapped air can have similar effect (Risser et al. 2005, Crosbie et al. 2005). The WTF method is calculated by multiplying the magnitude of water level change in wells by the specific yield of the aquifer material (Lee et al. 2006).

- $R = \Delta h / \Delta t \times S_y$ (5)

Where, R = recharge, S_y = specific yield.

Δh = change in water table height and it is extracted from the difference in maximum and minimum water level recorded on the hydrograph.

Δt = rise time, which is a year in this study. Thus, recharge was computed annually.

The accuracy of WTF is limited by the value of specific yield used because it was applied uniformly to the area. Since the value of specific yield varies with elevation, therefore, assuming

a constant value leads to errors in the recharge measured (Risser et al. 2005). Nonetheless the WTF represent a plausible estimate of recharge.

4 RESULTS

4.1 Hydrogeological framework

The GPR was used to map the subsurface configuration underlying the surficial aquifer. The GPR results shows a continuous clay confining bed below the surficial aquifer in the area, except in isolated areas where the confining layer is absent. The depth to the confining layer was extracted from each of the GPR profiles at a 100-feet distance interval and entered a database for statistical analyses. The statistical summary of the depth from the clay confining layer from the GPR radargram is shown in Table 4.1.

Table 4.1: Statistical distribution of the depth to confining layer mapped on the GPR profiles

Profile ID	**12**	**13**	**26**	**28**	**30**	**31**	**ALL**
Minimum	22.0	20.0	22.5	22.5	23.0	20.0	20.0
10^{th} Percentile	22.4	20.0	25.0	25.0	24.4	22.2	22.0
Median	25.0	25.0	25.0	25.0	25.0	24.5	25.0
90th Percentile	26.3	25.5	27.3	26.6	26.0	25.0	26.0
Maximum	27.5	27.0	27.5	27.5	27.5	25.0	27.5
Standard Dev.	2.0	2.3	1.1	1.2	1.5	1.2	1.8
Mean	24.2	23.7	25.1	25.2	25.0	23.8	24.4
n =	9	36	22	17	18	15	117
Profile Distance (ft)	1,540	6,180	2,175	1,645	1,870	1,430	14,840
Profile Dist. (miles)	0.29	1.17	0.41	0.31	0.35	0.27	2.81

The confining layer was mapped in parts of the study area except on profiles 12 and 13, where the GPR signals were strongly attenuated, this attenuation is likely due to saltwater intrusion occurring at the margins of the island-marsh boundary, as reported by Marshall (2019) who had earlier identified the controls on saltwater intrusion around the site. The depth to the confining beds were mapped at an approximate depth range between 24-27.5 ft and a median value of 25 ft beneath land surface (Figure 4.1).

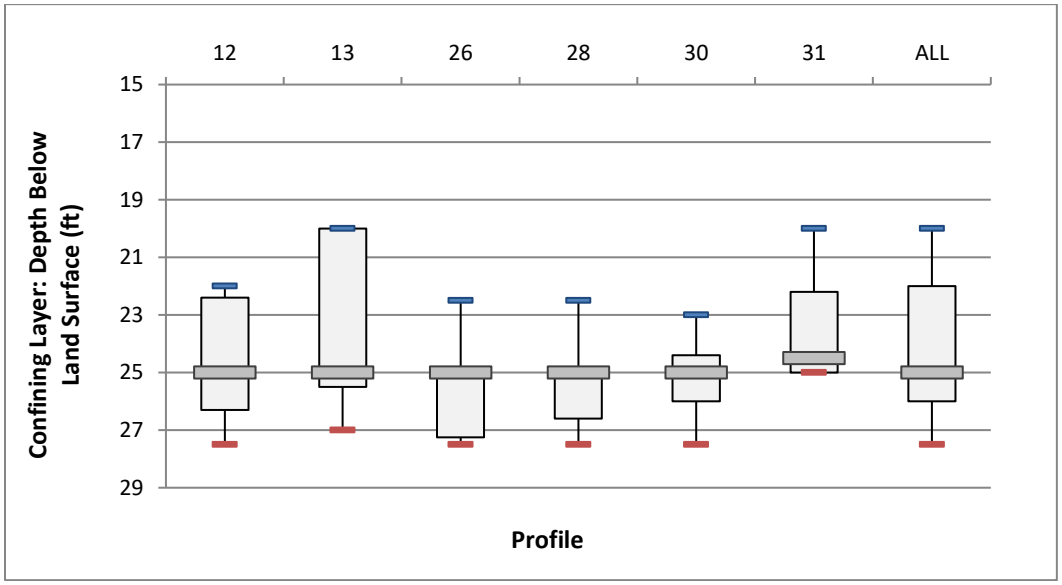

Figure 4.1: Box and whisker plot showing the statistical distribution of the depth to the confining layer extracted from the GPR data in the study area.

4.2 Porosity estimate

According to the equation 1 listed in section 2.1 and the procedure described, the values of total porosity and bulk density measured from the three repacked samples are summarized in Table 4.2. The mean porosity of 40.9 % was used in further computation in this study.

Table 4.2: Summary of the porosity testing results of the repacked samples.

Sample ID	Location	Dry Mass (g)	VOL_{solid} (cm^3)	$MASS_{sat}$ (g)	$MASS_{water}$ (g)	VOL_{total} (cm^3)	$Porosity_{total}$	BULK DENSITY (g/cm^3)
1	MW-04 (-9' BLS)	134.42	50.72	169.09	34.67	85.39	40.6%	1.57
2	MW-04 (-12' BLS)	132.13	49.86	165.88	33.75	83.61	40.4%	1.58
3	MW-03 (-15' BLS)	120.04	45.3	152.63	32.59	77.89	41.8%	1.54

Note:

1. VOL_{solid} = dry mass (g) divided by 2.65 g/cm3.

4.3 Total availability of water and annual recharge

The equation described in section 3.3 was used to construct the water table elevation raster image of the study area. The resulting water table elevation of the area ranges from -0.5 ft to 16.5 ft across the study area. The areas with higher elevation are shown in red color while the lesser elevation areas are in green (Figure 4.2).

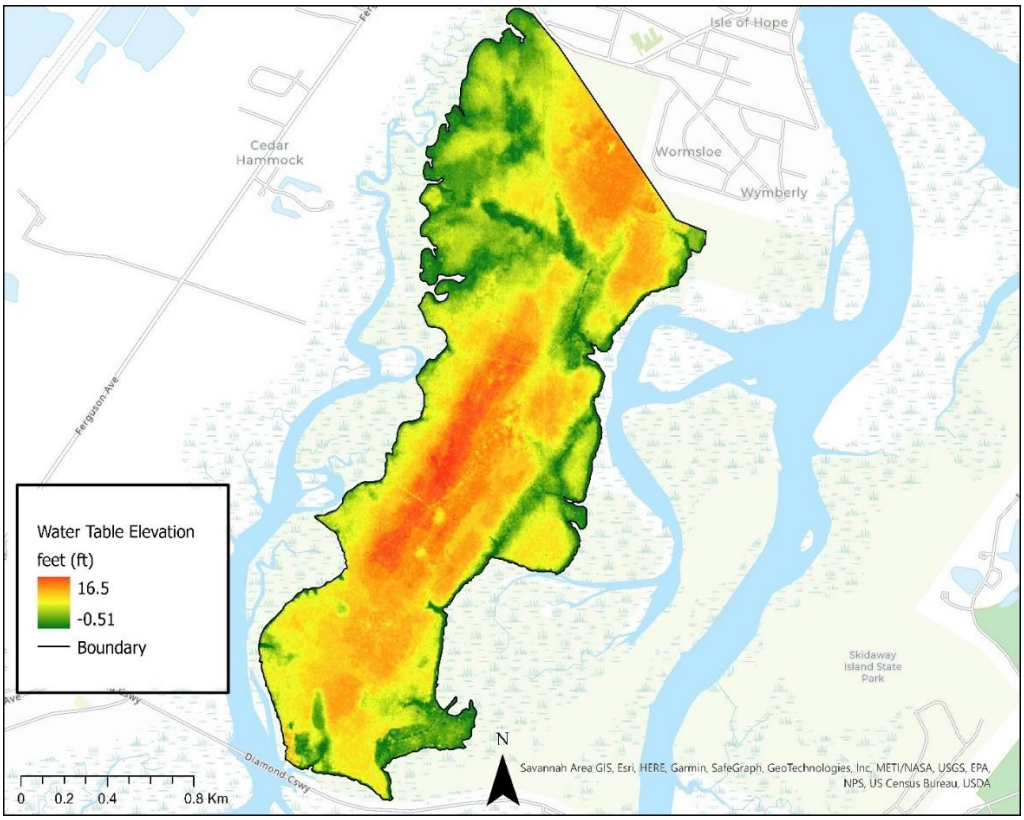

Figure 4.2: Estimated water-table elevation constructed from LIDAR and GPR data for Wormsloe Historic site.

Long-term water level data collected at the coastal groundwater monitoring network operated by the Department of Geosciences at Georgia State University, was used to construct a hydrograph which helped in identifying the seasonal high water table (SHWT) and seasonal low water table (SLWT) depth. The magnitude of seasonal fluctuations over a three-year period recorded by the hydrograph were found to be at a mean value of 2.50 ft and 4.00 ft below land surface. The result indicates an approximate 1.50 feet magnitude decline in water table depth between the summer and winter season in the study area (Figure 4.3).

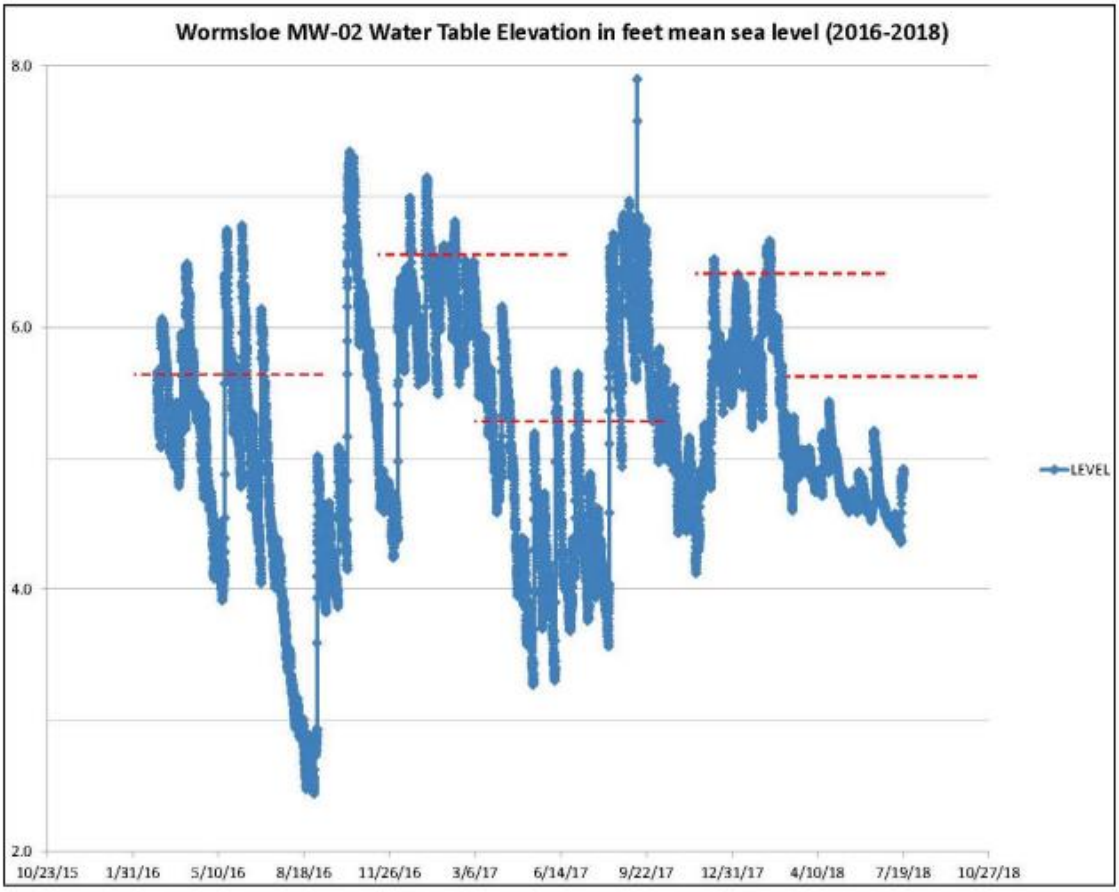

Figure 4.3: Long-term water level data from Wormsloe site Level transducer (Hodges, 2019). The water levels were recorded in MW-02 from 2016 -2018.

The mean seasonal high and low values were found to be at 2.50 ft and 4.00 ft, respectively. These values were subtracted from the surface elevation data (from Equation 2) to construct the SHWT and SLWT maps of the area. The SHWT and SLWT are presented in Figures 4.4 and 4.5.

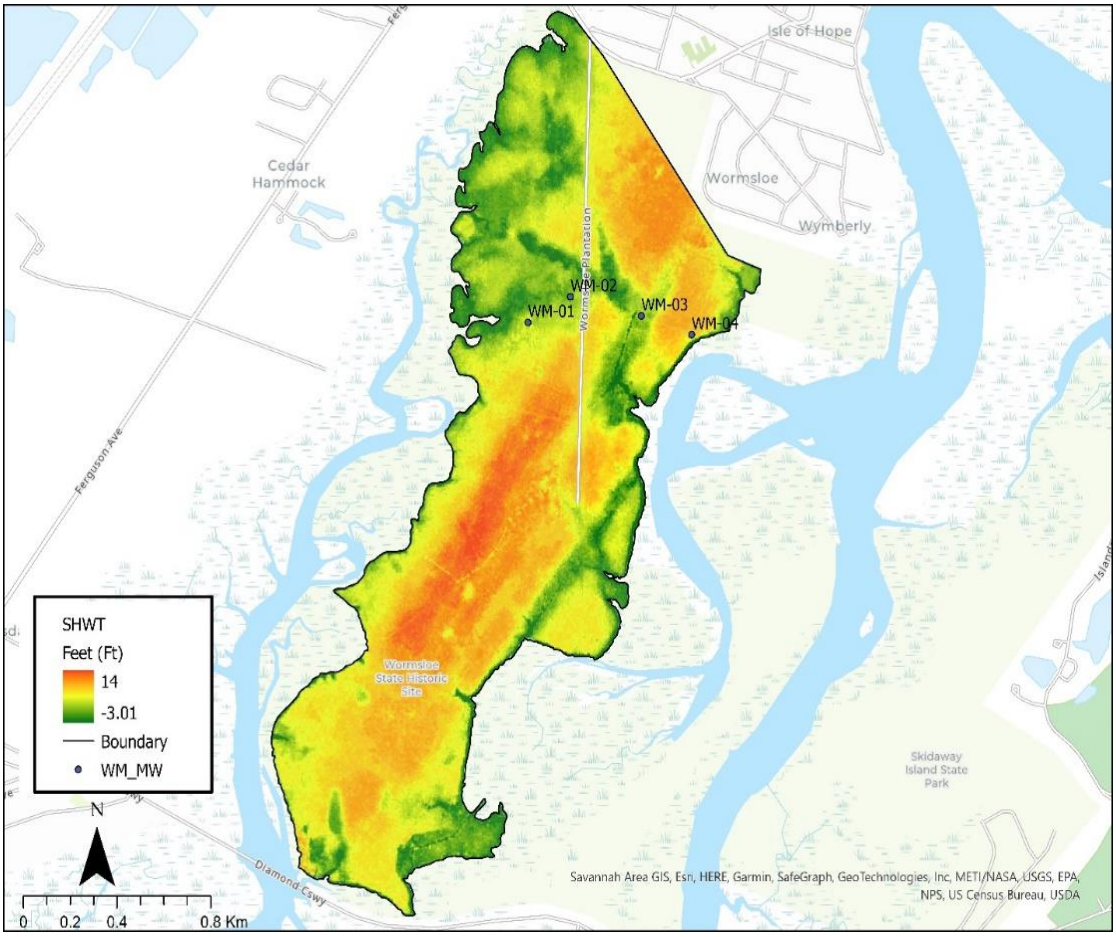

Figure 4.4: Seasonal high water table (SHWT) map of Wormsloe Historic site.

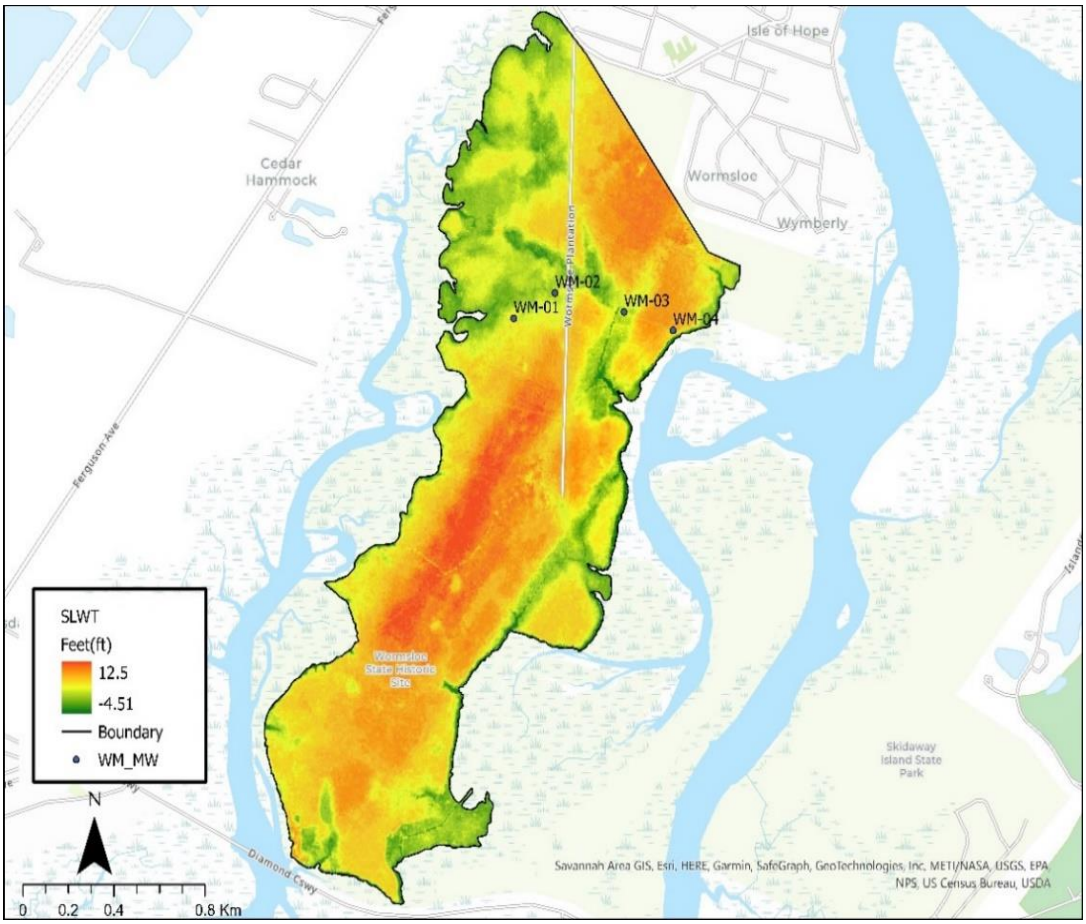

Figure 4.5: Seasonal low water table (SLWT) map of Wormsloe Historic site.

The saturated volume of water in the surficial aquifer under SHWT is estimated to be seven hundred and twenty-nine million cubic feet and about six hundred and eighty-two million cubic feet under SLWT conditions. The change in magnitude of the of saturated volume under both conditions were estimated and shows a difference of about forty-six million cubic feet. The total porosity from the laboratory estimates was used to determine the volume of void or porosity in which water are stored. The porosity value reveals that only 40.9% of the aquifer has void spaces to store fluids and was used to estimate the total volume of water in the storage. While the effective porosity of 0.36 was used based on the estimation that effective porosity ranges from 90-94 % of total porosity for unconsolidated sand (Hudak, 1994).

An approximate value of two hundred and ninety-eight million cubic feet of water was estimated under the SHWT. And about two hundred and seventy-nine million cubic feet under SLWT conditions. The change in total water availability in the aquifer is about 18 million cubic feet under both seasonal conditions. The volume of water available for pumping is approximately one hundred and seven million cubic feet and one hundred million cubic feet under both SHWT and SLWT conditions (Table 4.3).

Table 4.3: Summary of total water storage and percentage change in storage.

	Saturated Volume, Vol_{Sat} (ft^3)	**Total Vol. (ft^3) = (Vol_{sat} * ø)**	**Volume drained= $ø_{eff}$ *Total Vol**
SHWT	729,016, 816.85	298,167,878.09	107,340,436
SLWT	682,976,754.35	279,337,492.53	100,561,497.3
Difference	46,040,062.50	18,830,385.56	6,778,938
Percentage change (%)	**6.31**	**6.31**	**6.31**

We evaluated annual recharge estimates using the specific yield value of 0.09 (9%), though no experiment was performed to derive this value, it was adapted from Coes et al. (2007), who conducted similar measurement in a shallow aquifer of North Carolina. The recharge calculated using the water level change recorded by MW-02 hydrograph as described in section 3.4.

The recharge estimate was calculated for 2016 and 2017, since 2018 has no complete annual water level record. The result of the annual recharge estimate is presented in Table 4.4.

Table 4.4: Summary of change in water level and annual recharge estimate between 2016-2017.

Year	**h_{max}**	**h_{min}**	**Δh (ft)**	**Specific yield (S_y)**	**Recharge(ft)**
2016	2.47	6.97	4.50	0.09	0.405
2017	3.21	7.10	3.89	0.09	0.35

5 DISCUSSION

5.1 Surficial aquifer hydrogeological framework

Through the interpretation of the GPR data, the configuration of the surficial aquifer system beneath the Wormsloe Historic Site was mapped. The results indicate a variable depth to the water table of the surficial aquifer with a clay bearing confining layer present in the study area, although the confining layer is missing in isolated portions of the study area. The GPR further shows that small-scale faulting of the confining layer has occurred in some areas, this may allow some mixing of water seeping into or from the underlying UFA, based on an earlier observation made by Vance et al. (2016) and complemented by Marshall (2019). The GPR signal were observed to be strongly attenuated in many parts of the study area, and this was attributed to conductive losses from saltwater intrusion (Figure 5.1).

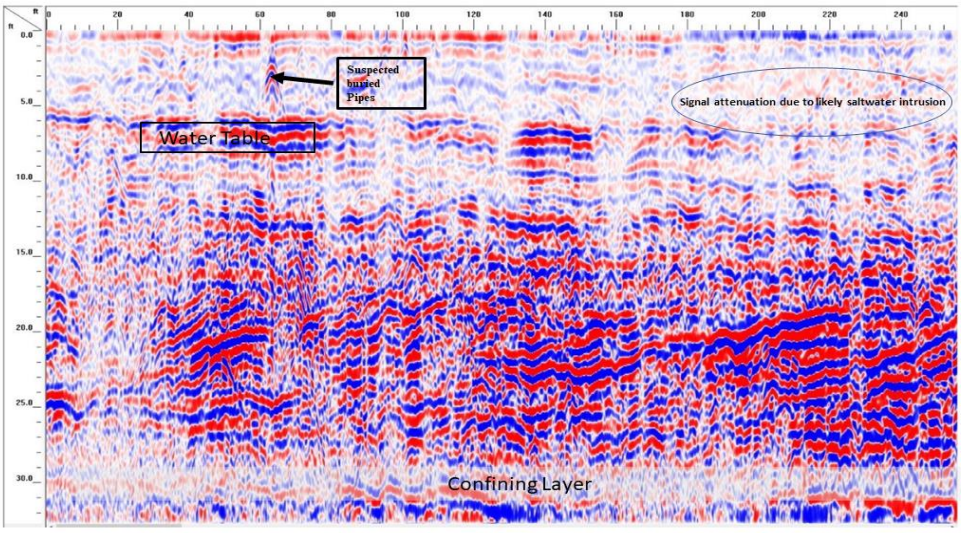

Figure 5.1: Processed GPR data from the 2021 data acquisition at Wormsloe site depicting the surficial aquifer system configuration and the accompanying signal attenuation recorded on the GPR section.

The signal attenuation is linked to seepage of saltwater intrusion through the fault structure, and this is particularly problematic in low elevation region along the edge of the island. This situation can be worsened due to the threat of sea-level rise (SLR). Since research has shown that alluvial plains and barrier island in coastal Florida are vulnerable to sea level rise (Xiao and Tang, 2019), and this situation may be similar for coastal Georgia. Thus, SLR may drive saltwater from the sea into areas with compromised structures such as faults and leaky aquitards (Payne, 2010) into the surficial aquifers in the study area. Therefore, saltwater intrusion may pose a challenge to the development of the surficial aquifer for landscape irrigation because saltwater is considered a threat to vegetation health.

5.2 Total availability of water and annual recharge estimates

The water table elevation map generated depict the changing elevation of the water table in the surficial aquifer across the study area. The result shows that the water table fluctuation

follows the pattern of the local topography. In addition, the water table elevation are further observed to be affected by local geology in some areas.

The total water storage in the surficial aquifer under both seasonal low and seasonal high conditions were estimated. The change in magnitude of about six (6) percent were observed under the SHWT and SLWT conditions in winter and summer season, respectively. The result supports the observation made by Karunarathne, (2022), who observed a reduction in water table elevation during the high tide in both wells (MW-03 and MW-04) in the summer season. The decrease in groundwater storage between the SHWT and SLWT can be ascribed to an increase in evapotranspiration, which has been observed in shallow aquifers of Southeastern U.S. (Condon et al. 2020)

The result implies that the effect of seasonal change in water table produces a magnitude reduction in water availability in the shallow groundwater in the area. Due to this, there would be a lesser volume of water to be withdrawn for landscape and agricultural irrigation in the area at the peak of summer which usually, is drier and hotter.

The major limitations to water availability in the surficial aquifer at Wormsloe as observed from the study is from the depletion in water storage occasioned by the changes in magnitude of SHWT and SLWT due to seasonal changes. In addition, the reported lateral intrusion of saltwater in parts of the shallow groundwater in Wormsloe will causes a reduction in water availability for non-potable uses in the study area. This observation is significant because in the summer season when water availability is low, this season has also been reported to have higher salt content (chloride concentration) than winter season (Karunarathne, 2022).

The recharge in the aquifer was estimated and found to vary between 0.35 ft and 0.40 ft for 2016 and 2017. The mean annual recharge for the two consecutive year under study (for a specific

yield of 0.09) is approximately 0.38 ft per year. This estimate is only indicative of the general recharge trend in the study area since recharge varies based on distribution and rainfall but provides a reference value for the area. It is noteworthy that specific yield value varies with elevation and using a constant value may introduce overestimation of recharge value.

5.3 Future research/Limitation of data

Future research should incorporate more representative samples for the estimation of porosity for accurate calculation of total water storage. In addition, the SHWT and SLWT conditions were evaluated based on two years historical well data. Longer term historical data will increase the accuracy in the estimation of volume of total water storage under both seasonal low and high conditions and further help quantify recharge more effectively. Future work will require more shallow monitoring wells in the area alongside salinity data to fully evaluate the zone of lateral saltwater intrusion in the area. Furthermore, there is a need to use pump test data to estimate the actual well yield alongside transmissivity in the study areas.

Future research can use a time lapse GPR data to assess the changes in the water table surface and compare with the monitoring well data to assess the uncertainties associated with using the GPR in characterizing water storage change. In addition, supplementary geophysical methods such as electrical resistivity and seismic refraction can be used to complement the GPR data in mapping water table depth. It can also help in delineating fault structure that could enhance the migration of saltwater intrusion into the surficial aquifer.

6 CONCLUSIONS

It is imperative to develop the surficial aquifer system in coastal areas of Georgia to support the growing population, agricultural activities, and to reduce reliance on the UFA and mitigate the effects of saltwater intrusion. Therefore, this research demonstrates that geophysical data via the GPR and the LIDAR derived DEM can be integrated to map the surficial aquifer in the areas. The results show that surficial aquifer can serve as alternative water resource based on the volume of total water storage estimates. The study further shows that there is a minimal effect of seasonal fluctuation on the surficial aquifer, therefore the surficial aquifer can be harnessed to support non-potable water demands, such as landscape irrigation which will help reduce the pressure on the deeper aquifers even in drier period.

However, based on the synthesis of the results in this study, there is a possibility of saltwater intrusion seeping into the surficial aquifer. Further study can therefore examine the driving force and the magnitude of the saltwater intrusions into the surficial aquifer. This study will help in future planning of groundwater resources and utilization.

REFERENCES

Annan, A.P. (2005). Ground-Penetrating Radar. Near-Surface Geophysics, Dwain K. Butler.

Barlow, P.M., Reichard, E.G.(2010). Saltwater intrusion in coastal regions of North America. Hydrogeology Journal **18,** 247–260 (2010). https://doi.org/10.1007/s10040-009-0514-3.

Berndt, M.P., Katz, B.G., Kingsbury, J.A., and Crandall, C.A. (2014). The quality of our Nation's waters—Water quality in the Upper Floridan aquifer and overlying surficial aquifers, southeastern United States, 1993–2010: U.S. Geological Survey Circular 1355, 72 p., http://dx.doi.org/10.3133/cir1355.

Bryan, J., Virginia S., Wood, and Mary R. Bullard.(1753). Journal of a Visit to the Georgia Islands of St. Catherines, Green, Ossabaw, Sapelo, St. Simons, Jekyll, and Cumberland, with Comments on the Florida Islands of Amelia, Talbot, and St. George, in 1753. Vol. 22. Mercer University Press, 1996.

Cherry, G.S. (2015) Groundwater flow in the Brunswick/Glynn County area, Georgia, 2000–04: U.S. Geological Survey Scientific Investigations Report 2015–5061, 88 p., http://dx.doi.org/10.3133/sir20155061.

Ciampoli LB, Tosti F, Economou N, Benedetto F. (2019). Signal processing of GPR data for road surveys. Geosciences. https://doi.org/10.3390/geosciences9020096.

Clarke, J.S. (2003). The surficial and Brunswick aquifer systems— Alternative ground-water resources for coastal Georgia, in Hatcher, K.J., ed., Proceedings of the 2003 Georgia Water Resources Conference, April 23–24, 2003: Athens, Georgia, The University of Georgia Institute of Ecology.

Clarke, J.S., Cherry, G.C., and Gonthier, G.J. (2011). Hydrogeology and water quality of the Floridan aquifer system and effects of Lower Floridan aquifer pumping on the Upper Floridan aquifer at Fort Stewart, Georgia: U.S. Geological Survey Scientific Investigations Report 2011– 5065, 59 p.

Cocker, M.D. (1999). Geochemical mapping in Georgia, USA: a tool for environmental studies, geologic mapping, and mineral exploration. Journal of Geochemical Exploration, Volume 67, Issues 1–3,1999,vPages 345-360,ISSN 0375-6742, https://doi.org/10.1016/S0375-6742(99)00079-

Coes, A.L., Spruill, T.B., Thomasson, M.J. (2006). Multiple-method estimation of recharge rates at diverse locations in the North Carolina Coastal Plain, USA. Hydrogeol. J. doi: 10.1007/s10040-006-0123-3

Condon, L. E., Atchley, A. L., & Maxwell, R. M. (2020). Evapotranspiration depletes groundwater under warming over the contiguous United States. Nature communications.

Conyers, L.B. (2004) Ground-Penetrating Radar for Archaeology. Alta Mira Press, Walnut Creek, 203 p.

Crosbie, R.S., Binning, P. and Kalma, J.D. (2005). A time series approach to inferring groundwater recharge using the water table fluctuation method. Water Resources. Res. 41, pp. 1–9.

Daniels, D.J. (1996) Surface-Penetrating Radar. The Institution of Electrical Engineering, London.

Daniels, D.J. (2004) Ground Penetrating Radar. 2nd Edition, IEE Radar, Sonar and Navigation Series 15 (Ed.). The Institution of Electrical Engineers, London.

Doolittle, J.A., Jenkinson, B., Hopkins, D., Ulmer, M., and Tuttle,W. (2006). Hydropedological

investigations with ground penetrating radar (GPR): Estimating water – table depths and local groundwater flow pattern in areas of course – textured soils. Geoderma 131 (2006) 317 – 329.

Engström, J., Praskievicz, S., Bearden, B., & Moradkhani, H. (2021). Decreasing water resources in Southeastern U.S. as observed by the GRACE satellites. *Water* Policy, **23**(4), 1017– 1029. https://doi.org/10.2166/WP.2021.039.

Essam, D., Ahmed, M., Abouelmagd, A., Soliman, F. (2020). Monitoring temporal variations in groundwater levels in urban areas using ground penetrating radar, Science of The Total Environment, Volume 703, 2020, 134986.

Falls, W.F., Ransom, C., Landmeyer, J.E., Reuber, E.J. and Edwards, L.E. (2005). Hydrogeology, water quality, and saltwater intrusion in the upper Floridan aquifer in the offshore area near Hilton Head Island, South Carolina, and Tybee Island, Georgia, 1999 - 2002, US Geological Survey, Scientific Investigations Report.

Freeze RA, Cherry JA (1979) Groundwater. Prentice-Hall, Englewood Cliffs, NJ, 604 pp.

Ganiyu, S.A., Oladunjoye, M.A., Onakoya, O.I. (2021). Combined electrical resistivity imaging and ground penetrating radar study for detection of buried utilities in Federal University of Agriculture , Abeokuta, Nigeria. 79:177 *Environ Earth Sci* **79,** 177 (2020). https://doi.org/10.1007/s12665-020-08919-2.

Guo, L., Chen, J., Cui, X., Fan, B., Lin, H. (2012). Application of ground penetrating radar for coarse root detection and quantification: a review. Plant Soil 362, 1–23 (2013).

Healy, R.W. and Cook, P.G. (2002) Using Groundwater Levels to Estimate Recharge. Hydrogeology journal, 10, 91-109. https://doi.org/10.1007/s10040-001-0178-0.

Healy, D., Katopodis, C. Tarrant, P. (2007). Application of Ground Penetrating Radar for River

Ice Surveys. CGU HS Committee on River Ice Processes and the Environment14th Workshop on the Hydraulics of Ice-Covered Rivers Quebec City, June 19 - 22, 2007.

Holden J, Burt TP and Vilas M. 2002. Application of ground-penetrating radar to the identification of subsurface piping in blanket peat. Earth surface processes and landforms 27:235-249.

Hudak, P.F. Effective porosity of unconsolidated sand; Estimation and impact on capture zone geometry. *Geo* **24,** 140–143 (1994). https://doi.org/10.1007/BF00767887.

Jassas, H., Merkel, B. (2014). Estimating Groundwater Recharge in the Semiarid Al-Khazir Gomal Basin, North Iraq. *Water* **2014**, *6*, 2467-2481. https://doi.org/10.3390/w6082467.

Johnson, D.G. (1992). Use Of Ground-Penetrating Radar for Water-Table Mapping, Brewster And Harwich, Massachusetts. U.S. Geological Survey Water-Resources Investigations Report 90-408.

Jordan, J. L. (2001). Negotiating water allocations using a comprehensive study format: the "tri-state water wars. Journal of Contemporary Water Research and Education 118 (1), 6.

Karki, R., Puneet S., Latif K., Subhasis M., Sarmistha S. (2021). Assessment of impact in groundwater levels and stream-aquifer interaction due to increased groundwater withdrawal in the lower Apalachicola-Chattahoochee-Flint (ACF) River Basin using MODFLOW, Journal of Hydrology: Regional Studies, Volume 34,2021,100802,ISSN 2214-5818 https://doi.org/10.1016/j.ejrh.2021.100802.

Karunarathne, G.S. (2022). Characterizing Temporal Dynamics of Isotope and Ion Chemistry in Groundwater Across a Barrier Island as Influenced by Rainfall and Tidal Cycles." Thesis, Georgia State University.

Khan, U. S. and Al-Nuaimy, W. (2010). Background removal from GPR data using Eigenvalues. Proceedings of the XIII International Conference on Ground Penetrating Radar, pp. 1-5, doi: 10.1109/ICGPR.2010.5550079.

Lancaster, R. I. (2017). Special Master Report FL v. GA No. 142.

Lee, C.H Chen, W.P., Lee, R.H. (2006). Estimation of groundwater recharge using water balance coupled with base-flow-record estimation and stable-base-flow analysis Environ Geol (2006) 51: 73–82 DOI 10.1007/s00254-006-0305-2.

Leucci, G., Negri, S., 2006. Use of ground penetrating radar to map subsurface archaeological features in an urban area. Journal of Archaeological Science - J ARCHAEOL SCI. 33. 502-512.10.1016/j.jas.2005.09.006.

Martinez, A, Byrnes, A.P. (2002). Modeling dielectric-constant values of geologic materials: an aid to ground-penetrating radar data collection and interpretation. Curr. Res. Earth Sci., 247 (2001), pp. 1-16.

Makkawi, M.H. (2004). Integrating GPR and geostatistical techniques to map the spatial extent of a shallow groundwater system, Journal of Geophysics and Engineering, Volume 1, Issue 1, March 2004, Pages 56–62, https://doi.org/10.1088/1742-2132/1/1/007.

Marella, R.L., and Berndt, M.P. (2005). Water withdrawals and trends from the Floridan aquifer system in the southeastern United States, 1950-2000: U.S. Geological Survey Circular 1278, 20 p.

Marella, R.L. (2009). Water withdrawals, use, and trends in Florida, 2005: U.S. Geological Survey Scientific Investigations Report 2009–5125, 49 p.

Maruddani, B., and Sandi, E. (2019). The Development of Ground Penetrating Radar (GPR) Data Processing. International Journal of Machine Learning and Computing, 9, 768-773.

Neto, P.X, Medeiros, W.M. (2006). A practical approach to correct attenuation effects in GPR data, Journal of Applied Geophysics, Volume 59, Issue 2,2006,Pages 140-151,ISSN 0926-9851,https://doi.org/10.1016/j.jappgeo.2005.09.002.

Oladeni, I.A. (2022). Rare-Earth Element Occurrences in Heavy Mineral Sand, Southeast Georgia. Thesis, Georgia State University, 2022. doi:https ://doi.org/10.57709/28900383.

Osinowo, O.O., Arowoogun, K.I. (2020). A multi-criteria decision analysis for groundwater potential evaluation in parts of Ibadan, southwestern Nigeria. *Appl Water Sci* **10,** 228. https://doi.org/10.1007/s13201-020-01311-2

Painter, J.A. (2019). Estimated use of water in Georgia for 2015 and water-use trends, 1985–2015: U.S. Geological Survey Open-File Report 2019–1086, 216 p., https://doi.org/10.3133/ofr20191086.

Payne, D.F. (2010). Effects of sea-level rise and pumpage elimination on saltwater intrusion in the Hilton Head Island area, South Carolina, 2004-2104. U.S. Geological Survey Scientific Investigations Report 2009-5251, 83 p.

Paz, C., Alcalá, F.J., Carvalho, J.M., Ribeiro, L. (2017). Current uses of ground penetrating radar in groundwater-dependent ecosystems research, Science of The Total Environment, Volume 595, 2017, Pages 868885, https://doi.org/10.1016/j.scitotenv.2017.03.210.

Porsani J., de Matos Jangelme G., and Kipnis R. (2012). Use of ground penetrating radar to map subsurface features at the Lapa do Santo archaeological site (Brazil). Near Surface Geophysics 10, 141–144.

Qablawi, B. (2016). A Comparison of Four Methods to Estimate Groundwater Recharge for Northeastern South Dakota. Electronic Theses and Dissertations. 957.

Reichard, J.S, Nelson, B.R, Meyer, B.K., and Vance, R.K. (2014). Evidence

For Saltwater Intrusion in The Upper Floridan Aquifer on St. Catherine's Island, Georgia. Southeastern Geology V. 50, No. 3, P. 109-122.

Risser, D.W. Gburek, W.J., and Gordon J. F. (2005). Comparison of Methods for Estimating Ground-Water Recharge and Base Flow at a Small Watershed Underlain by Fractured Bedrock in the Eastern United States Scientific Investigations Report 2005-5038. U.S. Department of the Interior U.S. Geological Survey.

Scanlon B.R., Healy R.W., Cook P.G. (2002). Choosing appropriate techniques for quantifying groundwater recharge. Hydrogeology Journal (in press). DOI 10.1007/s10040-001-0176-2.

Sophocleous, M.A. (1991) Combining the soil-water balance and water-level fluctuation methods to estimate natural groundwater recharge: practical aspects. Journal of Hydrology 124:229–241.

Smith, D. G., and Jol, H. M. (1992). Ground-penetrating radar investigation of a Lake Bonneville Delta, Provo level, Bringham City, Utah, Geology, 20, 1083-1086.

Vance, R. Kelly, Meyer, Brian K., and Reichard, James S. (2016). Structural Controls on the Hydrology of Two Georgia Barrier Islands. Southeastern Section Geological Society of America, 65th Annual Meeting, Columbia, SC.

Williams, M. D. (2019). Controls on Saltwater Intrusion in a Shallow Coastal Aquifer: Wormsloe Historic Site, GA. Thesis, Georgia State University.

Wilson, S.G., & Fischetti, T.R. (2010). Coastline Population Trends in the United States: 1960 to 2008. U.S. Census Bureau, U.S. Department of Commerce, Publication P25-1139, pp.1-27.

Xiao, H., Tang, Y. (2019). Assessing the “superposed” effects of storm surge from a Category 3 hurricane and continuous sea-level rise on saltwater intrusion into the surficial aquifer in coastal east-central Florida (USA). Environment Science Pollution Research **26,** 21882–21889 (2019). https://doi.org/10.1007/s11356-019-05513-3.

Zowam, F. (2020). Sustainability Evaluation of Shallow Groundwater for Non-potable Use, GSU Downtown Campus, Atlanta, Georgia." Thesis, Georgia State University, 2020.